Title: Simultaneous dual recordings from vestibular hair cells and their calyx afferents demonstrate multiple modes of transmission at these specialized endings
.

Running title: Three modes of synaptic transmission between vestibular Type I hair cells and calyx afferents

Authors: Donatella Contini[1], Gay R. Holstein[2,3] and Jonathan J. Art[1]

[1]Department of Anatomy & Cell Biology, University of Illinois College of Medicine, 808 S. Wood St, Chicago, IL 60612, USA. [2]Neurology and [3]Neuroscience, Icahn School of Medicine at Mount Sinai, 1468 Madison Ave, New York, NY 10029, USA.

Corresponding Author: jart@uic.edu

Abstract

In the vestibular periphery, transmission via conventional synaptic boutons is supplemented by postsynaptic calyceal endings surrounding Type I hair cells. This review focusses on the multiple modes of communication between these receptors and their enveloping calyces as revealed by simultaneous dual-electrode recordings. Classic orthodromic transmission is accompanied by two forms of bidirectional communication enabled by the extensive cleft between the Type I hair cell and its calyx. The slowest cellular communication low-pass filters the transduction current with a time constant 10 — 100 milliseconds: potassium ions accumulate in the synaptic cleft, depolarizing both the hair cell and afferent to potentials greater than necessary for rapid vesicle fusion in the receptor and potentially triggering action potentials in the afferent. On the millisecond timescale, conventional glutamatergic quantal transmission occurs when hair cells are depolarized to potentials sufficient for calcium influx and vesicle fusion. Depolarization also permits a third form of transmission which occurs over tens of microseconds, resulting from the large voltage- and ion-sensitive cleft-facing conductances in both the hair cell and the calyx that are open at their resting potentials. Current flowing out of either the hair cell or the afferent divides into the fraction flowing across the cleft into its cellular partner, and the remainder flowing out of the cleft and into the surrounding fluid compartment. These findings suggest multiple biophysical bases for the extensive repertoire of response dynamics seen in the population of primary vestibular afferent fibers. The results further suggest that evolutionary pressures drive selection for the calyx afferent.

Key words: synaptic transmission, hair cell, calyx, ion accumulation, quantal transmission, nonquantal transmission, ephaptic transmission, resistive coupling, vestibular

Introduction

A persistent question in vestibular research is the functional significance of specialized calyx endings present on a subset of primary afferents in vestibular end organs. A majority of afferent and all efferent synapses involving hair cells (HCs) in the labyrinth and cochlea are mediated by conventional bouton endings. While the calyx represents a unique characteristic distinguishing vestibular from auditory sensory epithelia, the function of this morphologically specialized synapse remains obscure. Recent dual simultaneous recordings from HCs and their associated calyx afferents demonstrate that there are three modes of intercellular communication between them. In addition to unidirectional quantal transmission from HCs to afferents, there are two bidirectional forms of transmission. The slower of the two results from potassium flux into the cleft from either HC or afferent over tens of milliseconds, which can elevate $[K^+]_{cleft}$ from a resting ~8 to >28 mM. The corresponding $E_{(K)}$ for channels facing the cleft are depolarized from -71 to -38 mV. The more rapid form of bidirectional transmission results from HC and afferent channels open near their respective resting potentials. These allow current flowing into the cleft from either HC or afferent to divide between a component flowing out of the cleft near its apex at the neck of the Type I HC and a component flowing across the cleft into the synaptic partner. As yet there is no compelling evidence that the calyx is uniquely associated with particular characteristics of afferent discharge regularity or dynamics.

Anatomy, synaptic morphology, and innervation

Vestibular epithelia of amniotes contain two HC receptor subtypes. These were initially differentiated by HC cytology alone, and were subsequently defined by morphological differences in their associated afferent processes as well (1). Type I HCs are flask-shaped and are innervated by an afferent chalice surrounding the entire basolateral HC surface except the apical neck. The extensiveness and exclusivity of the cleft between the HC and its enveloping calyx, together with the tight junction seal protecting the endolymphatic space, creates a unique, diffusion-limited, femtoliter environment that is markedly different from perilymph. Type II HCs are cylindrical and participate in comparatively small synapses involving bouton-like endings of vestibular afferents that terminate on the receptor somata and the outer calyceal faces (2, 3).

Both vestibular HC subtypes utilize ribbon synapses for quantal transmission. These structures were originally recognized in retinal photoreceptors, where the ribbons were bedecked with synaptic vesicles, a few of which attached to the cell's plasma membrane (4-8). Subsequent studies revealed variability in their overall structure (9, 10), resulting in the adoption of the more general term "synaptic body" to describe synaptic vesicles tethered to a central structure with a minority docked at an active zone.

Synaptic bodies have been reported in retinal photoreceptors and bipolar cells, pinealocytes, electroreceptors, and auditory and vestibular HCs (9). Both the morphology of the synaptic body, and the number, density, tethering and docking of the associated synaptic vesicles (10, 11) vary. In auditory HCs, this morphological diversity has been correlated with functional differences in peripheral auditory signal processing based on Ca^{2+}-dependent exocytosis (12, 13). In both vestibular and auditory HCs, ribbon synapse morphology is thought to underlie the ability of HCs to respond with graded, high rates of sustained quantal transmitter release (14, 15). This dual function is achieved by the orchestrated availability of

docked vesicles for immediate exocytosis, and tethered vesicles (the “readily releasable pool”) poised for imminent release (16, 17). As shown in Figure 1, ribbon synapses are present at Type I HC synapses with calyces, and Type II HC synapses with both boutons and calyx outer faces (2, 3, 18, 19). Efferent synapses with afferents and Type II HCs display conventional presynaptic membrane specializations and postsynaptic subsynaptic cisterns in the HCs. Despite this well-defined anatomy, however, the precise role of the calyx in shaping HC-afferent signaling is not known. In that context, it is noteworthy that Wersäll reportedly regretted his sequential naming of the HCs, deeming the Type I HC-calyx architecture more highly evolved (20).

Morphophysiology

Decades of effort has focused on mapping morphological attributes of vestibular end organs and correlating these maps with dynamics and statistics of afferent firing (21-29); (Review: (30)). Based on intracellular recordings, dye injections and light microscopic reconstructions (31, 32), the crista ampullaris in multiple species has been subdivided into concentrically or linearly organized zones that evince differences in HC demographics and afferent innervation patterns (33, 34) (Fig. 1D). The posterior canal crista of turtles, for example, is organized into two symmetrical hemicristae separated by a central torus (35, 36). Each hemicrista has a central zone surrounded by a peripheral area that extends toward the torus and planum. All afferents in the central zone have calyces, manifest as either calyx-only fibers (32, 33) or dimorphic (37) fibers having both calyx and bouton endings. Afferents with bouton terminals are present in the peripheral zones throughout the crista, but more densely populate the zone with larger afferent fibers nearest the torus (32). Reflecting this, Type I HCs are more prevalent in the central zone while Type II HCs are present throughout the crista.

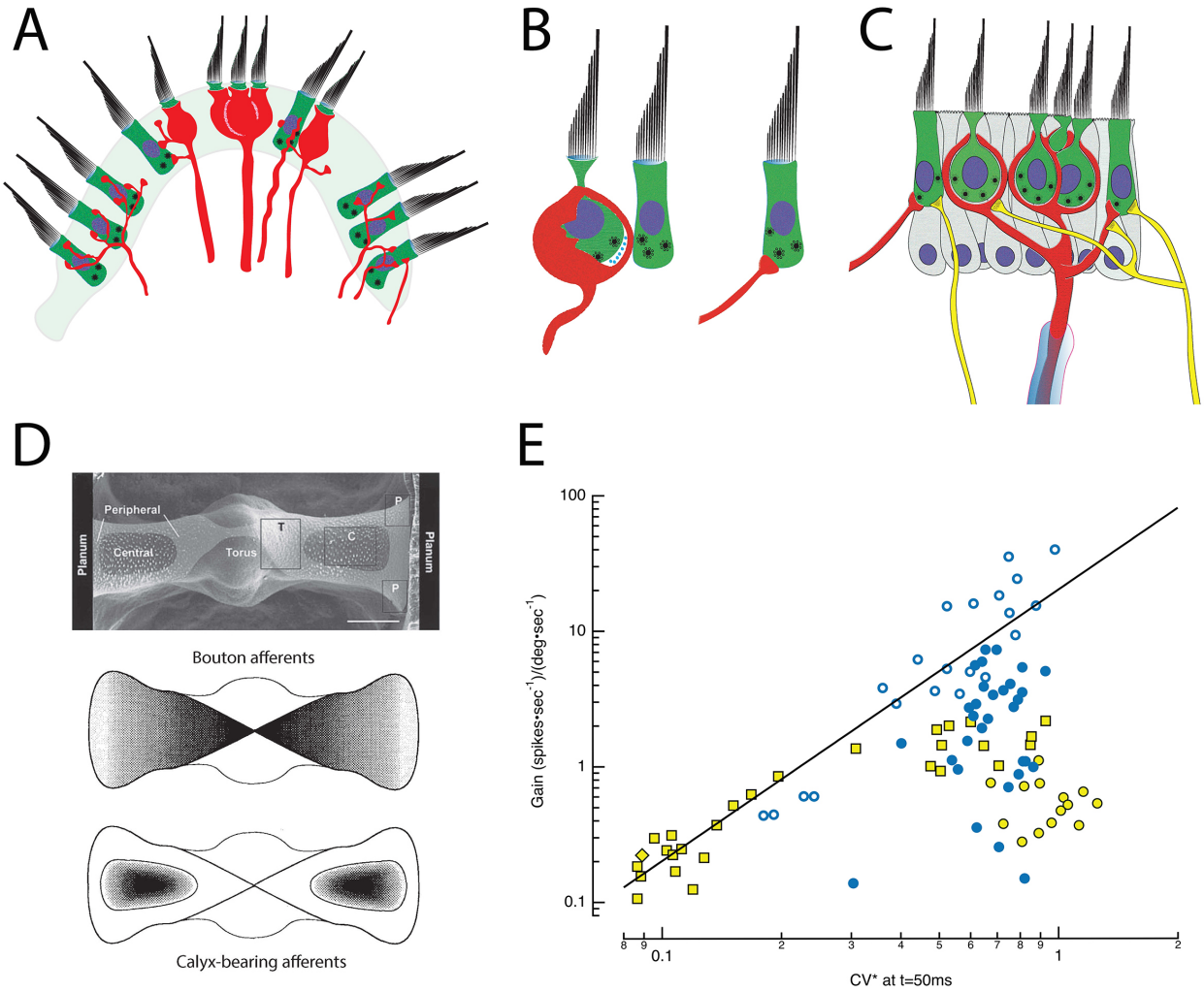

Figure 1. Morphophysiology of the semicircular canal (SCC) epithelium. A. Cross section through the saddle-shaped crista reveals distinct innervation patterns: boutons are found peripherally, with calyx and dimorphic afferents located centrally (adapted from (32)). B. Type I HCs are internal to an enveloping calyx that creates an extensive synaptic cleft in which ions accumulate. Type I HCs have synaptic bodies associated with quantal transmission onto the inner leaflet of the calyx. Type II HCs also have synaptic bodies indicative of quantal transmission, and synapse onto bouton endings (right) or onto the outer leaflet of an afferent calyx (middle and left). C. A single myelinated afferent (center, red) may branch into several calyces, each containing one or more Type I HCs. Additional input from Type II HCs may occur via synapses onto the outer face of the afferent (left), or through bouton endings of fine collateral branches (right). Efferent fibers (yellow) from the brainstem synapse on HCs and on the outer faces of calyces (60). D. Top: SEM plan view of the turtle posterior SCC (84). The epithelium is divided into two hemicristae with central and peripheral regions that extend bilaterally from the torus to the planum on either side. Middle: Map of the density of bouton afferents in each hemicrista. Bottom: Density map of the distribution of calyx-bearing afferents in the central regions of each hemicrista (36). E. Afferent signaling dynamics and discharge statistics in the posterior SCC of chinchilla (yellow symbols) (31) and turtle (blue symbols) (32) are correlated and map systematically across the epithelia. CV*, a measure of the irregularity of the interval between successive APs, is a continuous variable with the most regular fibers on the left and the most irregular on the right. Typically, when either animal was examined with low-frequency, 0.3 or 2 Hz, rotations, low gain afferents sensitive to velocity are more

regular, and high gain afferents are sensitive to accelerations. For the chinchilla, the low gain bouton (yellow diamond) and dimorphic (yellow square) afferents demonstrate that regular discharge can be achieved with either bouton or calyx endings. Data seen on the right side, including high gain bouton (turtle: blue, open circle) and dimorphic (turtle: blue, filled circle; chinchilla: yellow square) fibers demonstrate that irregular discharge can be achieved by afferents containing either type of ending. The irregular low gain "calyx only" afferents in chinchilla (yellow filled circle) remain a puzzle but may simply be afferents that respond maximally to stimulations at higher frequencies (49) or with vibration (114). CV* for chinchilla data transformed from 15 ms inter-spike interval (ISI) CV* to that at 50 ms ISI using a third-order polynomial fit to the CV* vs ISI data at 50 ms in Fig. 1 of (31), equivalent to the CV* and ISI used in the turtle data (32).

This differential localization of HCs and afferent endings across the crista underlies a coherent physiological and functional map of afferent activity (31, 33, 38-42). Specifically, the regularity of afferent fiber discharge, defined by the variability in time between sequential action potentials (APs) reportedly is a continuous variable correlating with the fiber's response to velocity or angular acceleration (43-46). Regular afferents have evenly spaced spontaneous firing rates and respond to low frequency angular motion with tonic discharge. In effect, this mathematically integrates the acceleration stimulus, transmitting signals that are proportional to head velocity. In contrast, the spontaneous firing of irregular afferents shows high variability in the timing between APs. Angular acceleration elicits phasic, dynamic responses from these fibers, which more closely resemble the accelerative stimulus. Moreover, regularly discharging fibers as a group have lower gain (spikes*sec^{-1}/degrees*sec^{-1}) than irregular afferents. In turtles, low gain, regularly-firing bouton afferent endings sensitive to velocity are concentrated near the planum, while higher gain bouton afferents sensitive to acceleration terminate closer to the torus (47). In contrast, most calyx-bearing fibers, which end in the central zone, are irregular afferents. The sensitivity of these fibers to low-frequency rotation varies over two orders of magnitude and is not strictly correlated with the degree of irregularity of the spontaneous discharge rate. Nevertheless, an integrated morphophysiological map of the crista emerges in which low gain, regularly discharging, velocity-sensitive bouton afferents terminate nearest the planum, bouton afferents of higher gain and more irregular discharge terminate nearest the torus, and calyx-bearing, irregularly-firing units terminate in the central zone of each hemicrista (Fig. 1D). Functionally, the high gain fibers across species are particularly attuned to acceleration (47) or to jerks, the derivative of acceleration (48), and rapidly saturate as the amplitude of the stimulus increases. Medium gain afferents remain active over a wider motion spectrum, while low gain fibers are not prone to saturate, regardless of the magnitude of the head acceleration (Fig. 1E). One caveat to this characterization is that the afferent gains were typically assessed at single low frequencies of stimulation (31, 32), although the most irregular fibers are often maximally responsive to higher frequencies and even vibrational or sound stimuli (49-51).

Based on the initial correlation of afferent terminal distribution with regularity of spontaneous firing and response dynamics, significant effort was directed toward identifying causality. It remained to be determined whether the regularity of a fiber's spontaneous firing derived from the geographical position of its terminals in the crista, or from the biophysical properties of HC inputs to trunk, branch, and twig segments of the parent process. Studies addressing this have been useful in highlighting the overall importance of regional localization

174 in the crista and suggesting the type of HCs, three-dimensional terminal architecture and
175 synapses contributing to individual afferent responses. However, efferent innervation (52-56),
176 GABA-mediated modulation of glutamatergic transmission (57-59), ion accumulation in the
177 synaptic cleft (60-63), and Type II HC input to the external face of the calyx (3, 64) have not
178 been incorporated into these analyses. Since each of these has the potential to markedly alter
179 peripheral vestibular activity, conclusions from these studies are necessarily tentative.
180

181 **Solitary cells**

182 To supplement information gleaned by morphophysiology, currents were analyzed from
183 HCs classified as Type I or II based on their amphoral or cylindrical profile (63, 65-83), from
184 identified regions of the epithelia (84). This approach emulated a strategy used in lower
185 vertebrates to demonstrate that the kinetics of voltage- and ion-sensitive basolateral channels
186 imparted frequency selectivity to solitary auditory HCs (85-91). Typically, solitary vestibular HCs
187 were bathed in artificial perilymph, an ionic environment appropriate for Type II cells, but of
188 unknown propriety for the ionically dynamic milieu of a Type I HC and its calyx. In principle,
189 such a bath would be apposite for isolating conductances based on their voltage ranges of
190 activation, kinetics, ionic permeabilities, and pharmacological profiles. In artificial perilymph
191 however, analysis of fundamental metrics such as I-V curves would be altered by driving forces
192 reflecting equilibrium potentials for each ion when bathed in high sodium and low potassium.
193 The vestibular potassium channels characterized in this way have been reviewed (92). A
194 startling discovery was that Type I HCs possess a low-voltage outward-rectifying potassium
195 current, $IK_{(LV)}$, that activates at very hyperpolarized potentials. Its full activation near the HC
196 resting potential was considered problematic, since enormous transduction currents would be
197 required to depolarize a cell to potentials necessary for the calcium influx and vesicle fusion
198 associated with quantal transmission. A solution to this paradox was proposed by Chen (93),
199 who suggested that potassium accumulation in the synaptic cleft between the HC and calyx was
200 analogous to the potassium accumulation in tissues surrounding the squid giant axon (94), and
201 that potassium flowing from the HC would increase $[K^+]_{cleft}$ and depolarize E_K for HC and
202 afferent conductances facing the cleft. As a result, the Type I HC would be depolarized at least
203 to potentials necessary for calcium influx and quantal transmission, but the increased $[K^+]_{cleft}$
204 would also depolarize the calyx.
205

206 **Theoretical and single-electrode studies**

207 Theoretical and experimental approaches were then used to examine the Chen conjecture.
208 The theoretical analysis (95, 96) relied on equivalent circuits of the Type I HC, cleft, and calyx to
209 analyze the problem primarily as ephaptic transmission (97-99) embellished by potassium
210 accumulation. In general, this analysis concluded that the potential drops associated with
211 current flow along the cleft from HC base to apex created only minor differences in the driving
212 force for channels facing the cleft, and as a result were not likely to be a major source of
213 coupling (96). The possibility that ion accumulation could have the effect suggested by Chen
214 was also examined experimentally (100). Following blockade of quantal transmission, slow
215 potentials that were phase-locked to the stimulus could be detected, a phenomenon consistent
216 with ion accumulation. Two groups examined the potassium accumulation question by
217 perforating the calyx and patch-recording from the enveloped Type I HCs *in situ* (101-103).

These experiments demonstrated that depolarization of either the HC or the calyx caused a reversal of the HC potassium tail currents, suggesting an elevation of $[K^+]_{cleft}$ consistent with Chen's conjecture. Such studies, together with one suggesting a transmitter role for protons (62), yielded results in which the interactions/coupling between cells occurred over tens of milliseconds. However, experiments using mechanical stimulation of the HC bundle demonstrated that when quantal transmission was blocked, the HC-afferent coupling could be extremely rapid, which would facilitate transmission of high frequency information (104, 105). Such contradictory viewpoints evoke the Indian parable of blind men describing an elephant (106), where each detects and interprets a small part of the more complex whole. This led to a quest to discover underlying biophysical mechanisms that could reconcile the differing results.

Dual-electrode studies

The demonstration that $[K^+]_{cleft}$ can be increased by potassium fluxes from either synaptic partner is a reminder that interpretations of single-electrode voltage-clamp studies of either HC or afferent alone can be problematic. The privileged ionic compartment created by the apposition between a HC and calyx means that any single-electrode study that voltage clamped one cell necessarily allowed the potential of the other cell to vary freely. Moreover, studies that patched onto Type I HCs *in situ* (101-105) did so by perforating the calyx, and there is ample evidence that this approach compromises the cleft environment and results in two types of recordings: those similar to solitary cells bathed in perilymph, and those in which reversal of the potassium tail currents demonstrate an increase in $[K^+]_{cleft}$ (101, 102).

To address this, we developed an approach to simultaneously patch the HC and calyx without breaching the inner calyceal membrane (60, 61). In essence, this requires patching the HC either on its apex or on the exposed 2 – 3µm of its basolateral wall extending apically above the enveloping calyx. With this approach, the potentials of both cells can be interrogated or controlled in current clamp or voltage clamp, leaving the cleft ionic environment intact.

Slow potassium accumulation depolarizes both HC and afferent to facilitate quantal transmission

Our initial studies (60) focused on ion accumulation and used the reversal potential of the HC potassium tail currents following depolarization to track E_K and estimate $[K^+]_{cleft}$. Blocking HC potassium flux abolished low-pass coupling of the transducer current occurring over tens of milliseconds, but spared quantal transmission. Our subsequent study (61) demonstrated that HC potassium flux depended upon the activation of both voltage-activated and calcium-activated potassium channels, and that the voltage-activated conductance was sensitive to $[K^+]_{cleft}$ and $[Ca^{2+}]_{cleft}$. Clamping $[H^+]_{cleft}$ resulted in stronger coupling between the two, suggesting that H^+ was not a primary transmitter acting through acid-sensitive ion channels. Pharmacological experiments using an HCN channel blocker (60) demonstrated that, in addition to synaptic coupling acting through HC and afferent potassium channels, the elevated $[K^+]_{cleft}$ not only decreased outward K^+ flux through calyceal voltage-sensitive potassium channels, but also shifted the activation curve of G_{HCN} (82), creating a depolarizing inward flux of Na^+ and K^+ through the HCN channels. These potassium-sensitive effects obtained regardless of whether the increased $[K^+]_{cleft}$ was due to HC or to afferent fluxes. Inward transduction currents would generate an outward flow of K^+ through the basolateral HC, elevate $[K^+]$ and shift E_K, causing depolarization of both HC and afferent (Fig 2A). Taken together, these results expand Chen's

263 conjecture that potassium accumulation in the cleft facilitates classical quantal transmission
264 between a Type I HC and calyx, and extend it to direct stimulation of the afferent as well. For
265 complex calyces with more than one enveloped HC, the findings indicate that depolarization of
266 one HC can depolarize the afferent, which would then depolarize neighboring receptors
267 enveloped by the shared afferent (Fig. 2A). In that light, slow potassium accumulation in the
268 cleft, above that in perilymph, is the ongoing leaky integration of transduction currents or
269 efferent excitation of the calyx, and thus can be interpreted as bidirectional inter-cellular
270 communication that acts over tens of milliseconds.
271
272 **HC and afferent depolarization creates resistive coupling through increased open-probability**
273 **of HC and afferent channels facing the cleft**
274 One remarkable result of these experiments (61) was a demonstration that there is also a
275 rapid bidirectional coupling between the cells that allows currents to activate within
276 microseconds of depolarization. With depolarization near the HC and calyx resting potentials,
277 there are a significant number of ion channels with high open probabilities. Rapid inward
278 transduction current would immediately flow out as potassium through HC channels, with
279 much of the current flowing into the extensive synaptic cleft and a minority flowing into the
280 calyx (Fig. 2B). Such coupling can be analyzed using either Kirchhoff's current or voltage laws,
281 and the conclusion is the same: there would be relatively small voltage gains or drops of a few
282 mV along the cleft depending on the current direction and the precise resistance (96, 107). The
283 impact of this on specific channels facing the cleft is unknown and would greatly depend on
284 their position with respect to the apical gap between HC and calyx. The dual recordings allow us
285 to measure the currents flowing out of one synaptic partner and into the other, or out through
286 the cleft (60, 61) (Fig. 2B, C). Such rapid current flow from HC into calyx, Fig. 2B, may underlie
287 the rapid transmission of high frequency mechanical stimuli (104, 105, 108), and may be the
288 substrate for detection of sound and vibration (26, 51, 109-115). As with slow potassium
289 accumulation, this rapid ion flow through open channels is bidirectional, as evidenced by the
290 retrograde transmission of calyx afferent APs into the HC (Fig. 2C) (60). Thus, as depolarization
291 persists, $[K^+]_{cleft}$ increases, and both the number of open channels and the amount of HC-
292 afferent electrical coupling increase concomitantly.
293 Dual recordings also provided the incidental observation that in the central region, the EPSCs
294 from Type I HCs onto the calyx inner leaflet were small (60, 116, 117), whereas those from
295 Type II HCs onto the outer leaflet (60) were as large as those reported in the cochlea (14), and
296 would be sufficient to trigger APs in afferents near the spike threshold. This highlights the risk
297 of morphophysiological studies defining calyx-only afferents based on light microscopy alone.

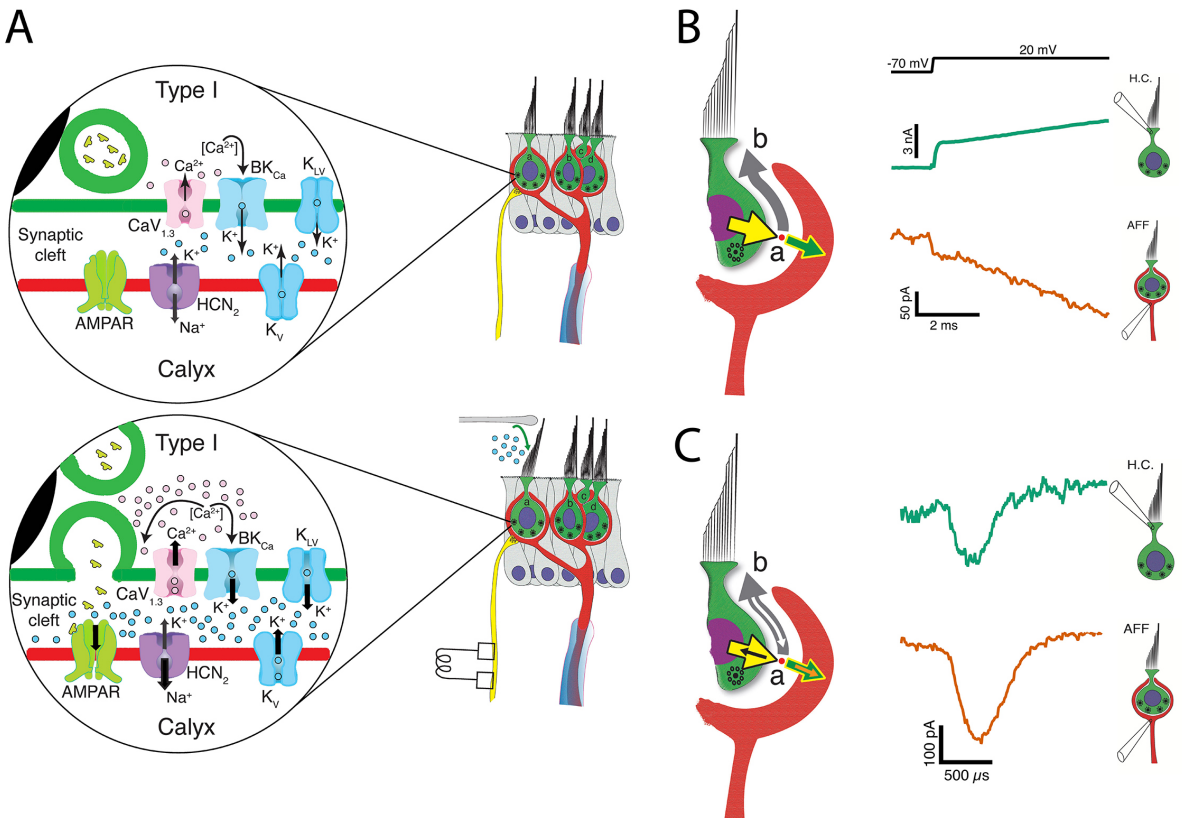

Figure 2. Three forms of synaptic transmission between a Type I HC and calyx afferent. A. In the absence of mechanical stimulation (upper panel), basolateral potassium currents activated at hyperpolarized potentials elevate the $[K^+]_{cleft}$ to concentrations near 8 mM, twice that found in perilymph. This results in a shift in E_K and depolarization of the HC to a resting potential between -60 and -50 mV, where $Ca_{1,3}$ channels are activated. At rest there is occasional vesicle fusion and the production of a background rate of afferent discharge. Upon mechanical stimulation (lower panel), the inward transduction current flows into the HC and out the basolateral conductances into the cleft as a potassium current. The further increase in $[K^+]_{cleft}$ is a low-pass integral of the transduction current and further depolarizes E_K for conductances in the HC and afferent membranes facing the cleft. The HC depolarization gates Ca^{2+} influx, resulting in fusion of synaptic vesicles and quantal transmission of glutamate to AMPARs on the calyx inner leaflet. The slow accumulation of potassium thereby facilitates quantal transmission near the resting potential, and for maintained depolarizations towards 0 mV, elevates $[K^+]_{cleft}$ to greater than 28 mM within 25 ms. It is likely that the irregularities of vesicle fusion and large quanta that initiate an AP are driven by neighboring Ca-channel noise (118), and as a consequence the degree of regularity of afferent discharge would be determined by the degree to which the post-synaptic afferent conductances have intrinsic memory and oscillatory behavior similar to those found in HCs of the turtle auditory papilla (89, 119). B. Large conductances in the HC and calyx near the resting potential also create an open resistive pathway between the two that permits a fraction of the transduction current to be communicated across the cleft and into the calyx without synaptic delay. Outward current from the HC (yellow arrow) divides at point (a) into a large component (gray arrow) going along the cleft into the bath at point (b), and a smaller current flowing into the calyx (green

arrow). The measured current for the HC (bluish-green current trace) and calyx (vermillion trace) show transmission within 10 µs. C. Resistive coupling can also be demonstrated during large HC depolarizations that depolarize the calyx to potentials sufficient to generate an AP that travels into the calyx. Currents due to the invasion of an AP will sum with the primary currents illustrated in B. With an AP, an additional inward current (orange arrow) flows into the calyx, with an amplitude equal to the sum of the corresponding currents flowing into the HC (black arrow) and down the cleft (white arrow). The coupling between the calyx retrograde AP current (vermillion) and the induced HC current (bluish-green) is 12 µs (modified from (61)).

Conclusions

During vertebrate evolution, selective pressures favored increased sensitivity and flawless encoding of three-dimensional vestibular information. This correlated with a higher prevalence of Type I HCs and calyx afferents (121, 122, 123, 134), which exhibit unidirectional quantal and two forms of bidirectional communication. Potassium accumulation in the synaptic cleft is a low-pass filter of HC transduction currents and afferent depolarizations by efferent fibers, and thus a leaky integrator of activity. At rest, $[K^+]_{cleft}$ is roughly 8 mM, or twice that found in perilymph, and is sufficient depolarize E_K and facilitate conventional quantal transmission. Maintained low-frequency excitation elevates $[K^+]_{cleft}$ further to >28 mM, a value sufficient to trigger afferent APs even in the absence of quantal transmission. From an evolutionary perspective, the pressure to extend transmission to higher frequencies was best served by direct resistive coupling created by large HC and afferent cleft-facing conductances present at and depolarized from rest. In evolving from bouton, through protocalyx to calyx, these conductances elevate $[K^+]_{cleft}$, depolarize E_K to facilitate quantal transmission, and provide a resistive path between synaptic partners that has minimal delay, is dynamic, and would increase as mechanical inputs become larger.

Author contributions

All authors have made a substantial, direct, and intellectual contribution to the work and approved it for publication.

Funding

This work was supported by NIH National Institute on Deafness and Other Communication Disorders grants R21 DC017292; R21 DC017577, R01 DC019953, and R01 DC008846

Acknowledgements

We would like to thank Professor A. Brichta for graciously allowing us to modify, reuse, and repurpose his figures in Figure 1.

References

1. Wersäll J. Studies on the structure and innervation of the sensory epithelium of the cristae ampullares in the guinea pig. *Acta Otolaryngology Suppliment (Stockh)* (1956) 126:7-85.
2. Goldberg JM, Lysakowski A, Fernández C. Morphophysiological and ultrastructural studies in the mammalian cristae ampullares. *Hear Res* (1990) 49(1-3):89-102. Epub 1990/11/01.

3. Lysakowski A, Goldberg JM. Ultrastructural analysis of the cristae ampullares in the squirrel monkey (Saimiri sciureus). *J Comp Neurol* (2008) 511(1):47-64. Epub 2008/08/30. doi: 10.1002/cne.21827.
4. Sjöstrand FS, editor. The Ultrastructure of the Retinal Rod Synapses of the Guinea Pig Eye. *Proceedings of the Electron Microscope Society of America*; 1953: Journal of Applied Physics (1953).
5. De Robertis E, Franchi CM. Electron microscope observations on synaptic vesicles in synapses of the retinal rods and cones. *J Biophys Biochem Cytol* (1956) 2(3):307-18. Epub 1956/05/25. doi: 10.1083/jcb.2.3.307.
6. Carasso N. Etude au microscope électronique des synapses des cellules visuelles chez le têtard d'Alytes obstetricans. [Electron microscopy of the synapses of the visual cells in the tadpole of Alytes obstetricans]. *Comptes rendus hebdomadaires des séances de l'Académie des sciences D, Sciences naturelles* (1957) 245(2):216-9. Epub 1957/07/08.
7. Polyak SL. *The Retina*. Chicago: The University of Chicago Press (1941).
8. Sjostrand FS. Ultrastructure of retinal rod synapses of the guinea pig eye as revealed by three-dimensional reconstructions from serial sections. *J Ultrastruct Res* (1958) 2(1):122-70. Epub 1958/11/01. doi: 10.1016/s0022-5320(58)90050-9.
9. Sterling P, Matthews G. Structure and function of ribbon synapses. *Trends Neurosci* (2005) 28(1):20-9. doi: 10.1016/j.tins.2004.11.009.
10. Moser T, Brandt A, Lysakowski A. Hair cell ribbon synapses. *Cell Tissue Res* (2006) 326(2):347-59. Epub 2006/09/01. doi: 10.1007/s00441-006-0276-3.
11. Schmitz F. The making of synaptic ribbons: how they are built and what they do. *Neuroscientist* (2009) 15(6):611-24. Epub 2009/08/25. doi: 10.1177/1073858409340253.
12. Johnson SL, Forge A, Knipper M, Munkner S, Marcotti W. Tonotopic variation in the calcium dependence of neurotransmitter release and vesicle pool replenishment at mammalian auditory ribbon synapses. *J Neurosci* (2008) 28(30):7670-8. doi: 10.1523/JNEUROSCI.0785-08.2008.
13. Meyer AC, Frank T, Khimich D, Hoch G, Riedel D, Chapochnikov NM, et al. Tuning of synapse number, structure and function in the cochlea. . *Nature Neurosci* (2009) 12:444–53.
14. Glowatzki E, Fuchs PA. Transmitter release at the hair cell ribbon synapse. *Nat Neurosci* (2002) 5(2):147-54. Epub 2002/01/22. doi: 10.1038/nn796.
15. Fuchs PA, Glowatzki E, Moser T. The afferent synapse of cochlear hair cells. *Curr Opin Neurobiol* (2003) 13(4):452-8. Epub 2003/09/11.
16. von Gersdorff H, Matthews G. Electrophysiology of synaptic vesicle cycling. *Annu Rev Physiol* (1999) 61:725-52. doi: 10.1146/annurev.physiol.61.1.725.
17. Holt M, Cooke A, Neef A, Lagnado L. High mobility of vesicles supports continuous exocytosis at a ribbon synapse. *Curr Biol* (2004) 14:173–83.
18. Lysakowski A, Goldberg JM. A regional ultrastructural analysis of the cellular and synaptic architecture in the chinchilla cristae ampullares. *J Comp Neurol* (1997) 389(3):419-43. Epub 1997/12/31.
19. Lysakowski A. Synaptic organization of the crista ampullaris in vertebrates. *Ann N Y Acad Sci* (1996) 781:164-82.
20. Engström H. The first-order vestibular neuron. In: Graybiel A, editor. *Symposium on the role of the vestibular organs in space exploration NASA SP-187*. Washington DC: National Academies (1970). p. 123-35.

21. Goldberg JM, Fernández C. Vestibular mechanisms. *Annu Rev Physiol* (1975) 37:129-62. Epub 1975/01/01. doi: 10.1146/annurev.ph.37.030175.001021.
22. Suzuki M, Harada Y. An experimental study on the frog semicircular canal--functions of cupula and vestibular ganglion. *J Otolaryngol* (1985) 14(1):36-40.
23. Suzuki M, Harada Y. An experimental study on the physiological significance of the mode of cupular movement. *Arch Otorhinolaryngol* (1985) 242(1):57-62.
24. Rabbitt RD, Boyle R, Highstein SM. Sensory transduction of head velocity and acceleration in the toadfish horizontal semicircular canal. *J Neurophysiol* (1994) 72(2):1041-8.
25. Hullar TE, Della Santina CC, Hirvonen T, Lasker DM, Carey JP, Minor LB. Responses of irregularly discharging chinchilla semicircular canal vestibular-nerve afferents during high-frequency head rotations. *J Neurophysiol* (2005) 93(5):2777-86. doi: 10.1152/jn.01002.2004.
26. Curthoys IS, Kim J, McPhedran SK, Camp AJ. Bone conducted vibration selectively activates irregular primary otolithic vestibular neurons in the guinea pig. *Exp Brain Res* (2006) 175(2):256-67. doi: 10.1007/s00221-006-0544-1.
27. Lasker DM, Han GC, Park HJ, Minor LB. Rotational responses of vestibular-nerve afferents innervating the semicircular canals in the C57BL/6 mouse. *J Assoc Res Otolaryngol* (2008) 9(3):334-48. doi: 10.1007/s10162-008-0120-4.
28. Jamali M, Sadeghi SG, Cullen KE. Response of vestibular nerve afferents innervating utricle and saccule during passive and active translations. *J Neurophysiol* (2009) 101(1):141-9. doi: 10.1152/jn.91066.2008.
29. Yu XJ, Dickman JD, Angelaki DE. Detection thresholds of macaque otolith afferents. *J Neurosci* (2012) 32(24):8306-16. doi: 10.1523/JNEUROSCI.1067-12.2012.
30. Paulin MG, Hoffman LF. Models of vestibular semicircular canal afferent neuron firing activity. *J Neurophysiol* (2019) 122(6):2548-67. Epub 2019/11/07. doi: 10.1152/jn.00087.2019.
31. Baird RA, Desmadryl G, Fernández C, Goldberg JM. The vestibular nerve of the chinchilla. II. Relation between afferent response properties and peripheral innervation patterns in the semicircular canals. *J Neurophysiol* (1988) 60(1):182-203. Epub 1988/07/01.
32. Brichta AM, Goldberg JM. Morphological identification of physiologically characterized afferents innervating the turtle posterior crista. *J Neurophysiol* (2000) 83(3):1202-23. Epub 2000/03/11.
33. Fernández C, Baird RA, Goldberg JM. The vestibular nerve of the chinchilla. I. Peripheral innervation patterns in the horizontal and superior semicircular canals. *J Neurophysiol* (1988) 60(1):167-81. Epub 1988/07/01.
34. Fernandez C, Lysakowski A, Goldberg JM. Hair-cell counts and afferent innervation patterns in the cristae ampullares of the squirrel monkey with a comparison to the chinchilla. *J Neurophysiol* (1995) 73(3):1253-69. Epub 1995/03/01.
35. Brichta AM, Peterson EH. Vestibular afferents innervating the posterior ampullae in a turtle, Pseudemys scripta. *Ann N Y Acad Sci* (1992) 656:914-6.
36. Brichta AM, Peterson EH. Functional architecture of vestibular primary afferents from the posterior semicircular canal of a turtle, Pseudemys (Trachemys) scripta elegans. *J Comp Neurol* (1994) 344(4):481-507. doi: 10.1002/cne.903440402.
37. Schessel DA, Highstein SM. Is transmission between the vestibular type I hair cell and its primary afferent chemical? *Ann N Y Acad Sci* (1981) 374:210-4.

38. Schessel DA, Ginzberg R, Highstein SM. Morphophysiology of synaptic transmission between type I hair cells and vestibular primary afferents. An intracellular study employing horseradish peroxidase in the lizard, Calotes versicolor. *Brain Res* (1991) 544(1):1-16.
39. Goldberg JM, Baird RA, Fernández C. Morphophysiological studies of the mammalian vestibular labyrinth. *Prog Clin Biol Res* (1985) 176:231-45. Epub 1985/01/01.
40. Fernández C, Goldberg JM, Baird RA. The vestibular nerve of the chinchilla. III. Peripheral innervation patterns in the utricular macula. *J Neurophysiol* (1990) 63(4):767-80. Epub 1990/04/01.
41. Goldberg JM, Desmadryl G, Baird RA, Fernández C. The vestibular nerve of the chinchilla. V. Relation between afferent discharge properties and peripheral innervation patterns in the utricular macula. *J Neurophysiol* (1990) 63(4):791-804. Epub 1990/04/01.
42. Goldberg JM, Desmadryl G, Baird RA, Fernández C. The vestibular nerve of the chinchilla. IV. Discharge properties of utricular afferents. *J Neurophysiol* (1990) 63(4):781-90. Epub 1990/04/01.
43. Fernández C, Goldberg JM. Physiology of peripheral neurons innervating semicircular canals of the squirrel monkey. II. Response to sinusoidal stimulation and dynamics of peripheral vestibular system. *J Neurophysiol* (1971) 34(4):661-75. Epub 1971/07/01.
44. Goldberg JM, Fernández C. Physiology of peripheral neurons innervating semicircular canals of the squirrel monkey. 3. Variations among units in their discharge properties. *J Neurophysiol* (1971) 34(4):676-84. Epub 1971/07/01.
45. Goldberg JM, Fernández C. Physiology of peripheral neurons innervating semicircular canals of the squirrel monkey. I. Resting discharge and response to constant angular accelerations. *J Neurophysiol* (1971) 34(4):635-60. Epub 1971/07/01.
46. Curthoys IS. The response of primary horizontal semicircular canal neurons in the rat and guinea pig to angular acceleration. *Exp Brain Res* (1982) 47(2):286-94. Epub 1982/01/01. doi: 10.1007/BF00239388.
47. Brichta AM, Goldberg JM. Responses to efferent activation and excitatory response-intensity relations of turtle posterior-crista afferents. *J Neurophysiol* (2000) 83(3):1224-42. Epub 2000/03/11.
48. Art JJ. Comparative physiology of primary afferents innervating semicircular canals in two species of plethodontid salamanders [Dissertation]: University of Chicago (1979).
49. Dickman JD, Correia MJ. Responses of Pigeon Horizontal Semicircular Canal Afferent Fibers II. High-Frequency Mechanical Stimulation. *J Neurophysiol* (1989) 62(5):1102-12.
50. McCue MP, Guinan JJ, Jr. Acoustically responsive fibers in the vestibular nerve of the cat. *J Neurosci* (1994) 14(10):6058-70.
51. Curthoys IS, Burgess AM, Goonetilleke SC. Phase-locking of irregular guinea pig primary vestibular afferents to high frequency (>250Hz) sound and vibration. *Hear Res* (2019) 373:59-70. Epub 2019/01/02. doi: 10.1016/j.heares.2018.12.009.
52. Poppi LA, Holt JC, Lim R, Brichta AM. A review of efferent cholinergic synaptic transmission in the vestibular periphery and its functional implications. *J Neurophysiol* (2019). Epub 2019/12/05. doi: 10.1152/jn.00053.2019.
53. Holt JC, Jordan PM, Lysakowski A, Shah A, Barsz K, Contini D. Muscarinic Acetylcholine Receptors and M-Currents Underlie Efferent-Mediated Slow Excitation in Calyx-Bearing Vestibular Afferents. *J Neurosci* (2017) 37(7):1873-87. doi: 10.1523/JNEUROSCI.2322-16.2017.

496 54. Holt JC, Kewin K, Jordan PM, Cameron P, Klapczynski M, McIntosh JM, et al.
497 Pharmacologically distinct nicotinic acetylcholine receptors drive efferent-mediated excitation
498 in calyx-bearing vestibular afferents. *J Neurosci* (2015) 35(8):3625-43. Epub 2015/02/27. doi:
499 10.1523/jneurosci.3388-14.2015.
500 55. Jordan PM, Parks XX, Contini D, Holt JC. A review of synaptic mechanisms of vestibular
501 efferent signaling in turtles: extrapolation to efferent actions in mammals. *J Vestib Res* (2013)
502 23(3):161-75. Epub 2013/11/02. doi: 10.3233/ves-130492.
503 56. Raghu V, Salvi R, Sadeghi SG. Efferent Inputs Are Required for Normal Function of
504 Vestibular Nerve Afferents. *J Neurosci* (2019) 39(35):6922-35. Epub 2019/07/10. doi:
505 10.1523/JNEUROSCI.0237-19.2019.
506 57. Holstein GR, Rabbitt RD, Martinelli GP, Friedrich VL, Jr., Boyle RD, Highstein SM.
507 Convergence of excitatory and inhibitory hair cell transmitters shapes vestibular afferent
508 responses. *Proc Natl Acad Sci U S A* (2004) 101(44):15766-71. doi: 10.1073/pnas.0402824101.
509 58. Holstein GR, Martinelli GP, Henderson SC, Friedrich VL, Jr., Rabbitt RD, Highstein SM.
510 Gamma-aminobutyric acid is present in a spatially discrete subpopulation of hair cells in the
511 crista ampullaris of the toadfish Opsanus tau. *J Comp Neurol* (2004) 471(1):1-10. doi:
512 10.1002/cne.11025.
513 59. Highstein SM, Rabbitt RD, Holstein GR, Boyle RD. Determinants of spatial and temporal
514 coding by semicircular canal afferents. *J Neurophysiol* (2005) 93(5):2359-70. doi:
515 10.1152/jn.00533.2004.
516 60. Contini D, Price SD, Art JJ. Accumulation of K+ in the synaptic cleft modulates activity by
517 influencing both vestibular hair cell and calyx afferent in the turtle. *J Physiol* (2017)
518 595.3(3):777-803. doi: 10.1113/JP273060.
519 61. Contini D, Holstein GR, Art JJ. Synaptic cleft microenvironment influences potassium
520 permeation and synaptic transmission in hair cells surrounded by calyx afferents in the turtle. *J*
521 *Physiology* (2020) 598.4(4):853-89. Epub 2019/10/18. doi: 10.1113/JP278680.
522 62. Highstein SM, Holstein GR, Mann MA, Rabbitt RD. Evidence that protons act as
523 neurotransmitters at vestibular hair cell-calyx afferent synapses. *Proc Natl Acad Sci U S A* (2014)
524 111(14):5421-6. doi: 10.1073/pnas.1319561111.
525 63. Chen JW, Eatock RA. Major potassium conductance in type I hair cells from rat semicircular
526 canals: characterization and modulation by nitric oxide. *J Neurophysiol* (2000) 84(1):139-51.
527 64. Ross MD, Rogers CM, Donovan KM. Innervation patterns in rat saccular macula. A structural
528 basis for complex sensory processing. *Acta Otolaryngol* (1986) 102(1-2):75-86. Epub
529 1986/07/01. doi: 10.3109/00016488609108649.
530 65. Valat J, Devau G, Dulon D, Sans A. Vestibular hair cells isolated from guinea pig labyrinth.
531 *Hear Res* (1989) 40(3):255-60. Epub 1989/07/01.
532 66. Masetto S, Russo G, Taglietti V, Prigioni I. [K+ and Ca++ currents in hair cells isolated from
533 the semicircular canals of the frog]. *Boll Soc Ital Biol Sper* (1991) 67(5):493-500.
534 67. Rennie KJ, Ashmore JF. Ionic currents in isolated vestibular hair cells from the guinea-pig
535 crista ampullaris. *Hear Res* (1991) 51:279-92.
536 68. Prigioni I, Masetto S, Russo G, Taglietti V. Calcium currents in solitary hair cells isolated
537 from frog crista ampullaris. *J Vestib Res* (1992) 2(1):31-9.
538 69. Griguer C, Kros CJ, Sans A, Lehouelleur J. Potassium currents in type II vestibular hair cells
539 isolated from the guinea-pig's crista ampullaris [published erratum appears in Pflugers Arch

1994 May;427(1-2):193]. *Pflugers Archiv European Journal of Physiology* (1993) 425(3-4):344-52.
70. Griguer C, Sans A, Lehouelleur J. Non-typical K(+)-current in cesium-loaded guinea pig type I vestibular hair cell. *Pflugers Archiv European Journal of Physiology* (1993) 422(4):407-9.
71. Griguer C, Sans A, Valmier J, Lehouelleur J. Inward potassium rectifier current in type I vestibular hair cells isolated from guinea pig. *Neurosci Lett* (1993) 149(1):51-5.
72. Lapeyre PN, Kolston PJ, Ashmore JF. GABAB-mediated modulation of ionic conductances in type I hair cells isolated from guinea-pig semicircular canals. *Brain Res* (1993) 609(1-2):269-76.
73. Rennie KJ, Ashmore JF. Effects of extracellular ATP on hair cells isolated from the guinea-pig semicircular canals. *Neurosci Lett* (1993) 160(2):185-9.
74. Rennie KJ, Correia MJ. Potassium currents in mammalian and avian isolated type I semicircular canal hair cells. *J Neurophysiol* (1994) 71(1):317-29. Epub 1994/01/01.
75. Ricci AJ, Cochran SL, Rennie KJ, Correia MJ. Vestibular type I and type II hair cells. 2: Morphometric comparisons of dissociated pigeon hair cells. *J Vestib Res* (1997) 7(5):407-20. Epub 1997/11/05.
76. Ricci AJ, Rennie KJ, Cochran SL, Kevetter GA, Correia MJ. Vestibular type I and type II hair cells. 1: Morphometric identification in the pigeon and gerbil. *J Vestib Res* (1997) 7(5):393-406. Epub 1997/11/05.
77. Eatock RA, Rusch A, Lysakowski A, Saeki M. Hair cells in mammalian utricles. *Otolaryngol Head Neck Surg* (1998) 119(3):172-81.
78. Marcotti W, Russo G, Prigioni I. Inactivating and non-activating delayed rectifier K+ currents in hair cells of frog crista ampullaris. *Hear Res* (1999) 135(1-2):113-23.
79. Martini M, Rossi ML, Rubbini G, Rispoli G. Calcium currents in hair cells isolated from semicircular canals of the frog. *Biophys J* (2000) 78(3):1240-54. doi: 10.1016/S0006-3495(00)76681-1.
80. Rennie KJ, Weng T, Correia MJ. Effects of KCNQ channel blockers on K(+) currents in vestibular hair cells. *Am J Physiol Cell Physiol* (2001) 280(3):C473-80. Epub 2001/02/15.
81. Li GQ, Meredith FL, Rennie KJ. Development of K(+) and Na(+) conductances in rodent postnatal semicircular canal type I hair cells. *Am J Physiol Regul Integr Comp Physiol* (2010) 298(2):R351-8. doi: 10.1152/ajpregu.00460.2009.
82. Meredith FL, Benke TA, Rennie KJ. Hyperpolarization-activated current (I(h)) in vestibular calyx terminals: characterization and role in shaping postsynaptic events. *J Assoc Res Otolaryngol* (2012) 13(6):745-58. doi: 10.1007/s10162-012-0342-3.
83. Mann SE, Johnson M, Meredith FL, Rennie KJ. Inhibition of K+ currents in type I vestibular hair cells by gentamicin and neomycin. *Audiol Neurootol* (2013) 18(5):317-26. doi: 10.1159/000354056.
84. Brichta AM, Aubert A, Eatock RA, Goldberg JM. Regional analysis of whole cell currents from hair cells of the turtle posterior crista. *J Neurophysiol* (2002) 88(6):3259-78. Epub 2002/12/06. doi: 10.1152/jn.00770.2001.
85. Lewis RS, Hudspeth AJ. Voltage- and ion-dependent conductances in solitary vertebrate hair cells. *Nature* (1983) 304(5926):538-41. Epub 1983/08/11.
86. Lewis RS, Hudspeth AJ. Frequency tuning and ionic conductances in hair cells of the bullfrog's sacculus. In: Klinke R, Hartmann R, editors. *Hearing-Physiological Bases and Psychophysics*. Berlin: Springer-Verlag (1983). p. 17-24.

87. Hudspeth AJ, Lewis RS. A model for electrical resonance and frequency tuning in saccular hair cells of the bull-frog, Rana catesbeiana. *J Physiol* (1988) 400:275-97. Epub 1988/06/01.
88. Hudspeth AJ, Lewis RS. Kinetic analysis of voltage- and ion-dependent conductances in saccular hair cells of the bull-frog, Rana catesbeiana. *J Physiol* (1988) 400:237-74. Epub 1988/06/01.
89. Art JJ, Fettiplace R. Variation of membrane properties in hair cells isolated from the turtle cochlea. *J Physiol* (1987) 385:207-42. Epub 1987/04/01.
90. Art JJ, Crawford AC, Fettiplace R. Electrical resonance and membrane currents in turtle cochlear hair cells. *Hear Res* (1986) 22:31-6. Epub 1986/01/01.
91. Smotherman MS, Narins PM. The electrical properties of auditory hair cells in the frog amphibian papilla. *J Neurosci* (1999) 19(13):5275-92.
92. Meredith FL, Rennie KJ. Channeling your inner ear potassium: K(+) channels in vestibular hair cells. *Hear Res* (2016). doi: 10.1016/j.heares.2016.01.015.
93. Chen W-Y. The Properties and Functions of a Low-Voltage Activated K(+) Current in Type I Hair Cells of Rat Semicircular Canal Organs [Dissertation]. Rochester, NY: University of Rochester (1995).
94. Frankenhaeuser B, Hodgkin AL. The after-effects of impulses in the giant nerve fibres of Loligo. *J Physiol* (1956) 131(2):341-76.
95. Goldberg JM. Transmission between the type I hair cell and its calyx ending. *Ann N Y Acad Sci - New Directions in Vestibular Research* (1996) 781:474-88. Epub 1996/06/19.
96. Goldberg JM. Theoretical analysis of intercellular communication between the vestibular type I hair cell and its calyx ending. *J Neurophysiol* (1996) 76(3):1942-57. Epub 1996/09/01.
97. Arvanitaki A. Effects evoked in an axon by the activity of a contiguous one. *J Neurophysiol* (1942) 5(2):89-108. doi: 10.1152/jn.1942.5.2.89.
98. Katz B, Schmitt OH. Electric interaction between two adjacent nerve fibres. *J Physiol* (1940) 97(4):471-88.
99. Kramer RH, Davenport CM. Lateral Inhibition in the Vertebrate Retina: The Case of the Missing Neurotransmitter. *PLoS Biol* (2015) 13(12):e1002322. Epub 2015/12/15. doi: 10.1371/journal.pbio.1002322.
100. Holt JC, Chatlani S, Lysakowski A, Goldberg JM. Quantal and nonquantal transmission in calyx-bearing fibers of the turtle posterior crista. *J Neurophysiol* (2007) 98(3):1083-101. Epub 2007/06/29. doi: 10.1152/jn.00332.2007.
101. Contini D. Intercellular K+ accumulation drives Type I hair cells into the activation range of voltage-gated Ca channels [Dissertation]. Pavia, Italy: University of Pavia (2011).
102. Contini D, Zampini V, Tavazzani E, Magistretti J, Russo G, Prigioni I, et al. Intercellular K(+) accumulation depolarizes Type I vestibular hair cells and their associated afferent nerve calyx. *Neuroscience* (2012) 227:232-46. doi: 10.1016/j.neuroscience.2012.09.051.
103. Lim R, Kindig AE, Donne SW, Callister RJ, Brichta AM. Potassium accumulation between type I hair cells and calyx terminals in mouse crista. *Exp Brain Res* (2011) 210(3-4):607-21. Epub 2011/02/26. doi: 10.1007/s00221-011-2592-4.
104. Eatock RA, Songer JE. Vestibular hair cells and afferents: two channels for head motion signals. *Annu Rev Neurosci* (2011) 34:501-34. doi: 10.1146/annurev-neuro-061010-113710.
105. Songer JE, Eatock RA. Tuning and timing in mammalian type I hair cells and calyceal synapses. *J Neurosci* (2013) 33(8):3706-24. Epub 2013/02/22. doi: 10.1523/jneurosci.4067-12.2013.

629 106. Ireland J. *The Udana & The Itivuttaka: Inspired Utterances of the Buddha & The Buddha's*
630 *Sayings*: BPS Pariyatti Editions (2020).
631 107. Govindaraju AC, Quraishi IH, Lysakowski A, Eatock RA, Raphael RM. A Biophysical Model of
632 Nonquantal Transmission at the Vestibular Hair Cell-Calyx Synapse: K(LV) currents Modulate
633 Fast Electrical and Slow K(+) potentials in the Synaptic Cleft. *bioRxiv* (2021):2021.11.18.469197.
634 doi: 10.1101/2021.11.18.469197.
635 108. Eatock RA. Specializations for Fast Signaling in the Amniote Vestibular Inner Ear. *Integr*
636 *Comp Biol* (2018) 58(2):341-50. Epub 2018/06/20. doi: 10.1093/icb/icy069.
637 109. McCue MP, Guinan JJ, Jr. Sound-evoked activity in primary afferent neurons of a
638 mammalian vestibular system. *Am J Otol* (1997) 18(3):355-60.
639 110. McCue MP, Guinan JJ, Jr. Spontaneous activity and frequency selectivity of acoustically
640 responsive vestibular afferents in the cat. *J Neurophysiol* (1995) 74(4):1563-72.
641 111. McCue MP, Guinan JJ, Jr. Influence of efferent stimulation on acoustically responsive
642 vestibular afferents in the cat. *J Neurosci* (1994) 14(10):6071-83. Epub 1994/10/01.
643 112. Curthoys IS, Vulovic V. Vestibular primary afferent responses to sound and vibration in the
644 guinea pig. *Exp Brain Res* (2011) 210(3-4):347-52. doi: 10.1007/s00221-010-2499-5.
645 113. Curthoys IS, Vulovic V, Sokolic L, Pogson J, Burgess AM. Irregular primary otolith afferents
646 from the guinea pig utricular and saccular maculae respond to both bone conducted vibration
647 and to air conducted sound. *Brain Res Bull* (2012) 89(1-2):16-21. doi:
648 10.1016/j.brainresbull.2012.07.007.
649 114. Curthoys IS, Grant JW. How does high-frequency sound or vibration activate vestibular
650 receptors? *Exp Brain Res* (2015) 233(3):691-9. doi: 10.1007/s00221-014-4192-6.
651 115. Curthoys IS, Vulovic V, Burgess AM, Sokolic L, Goonetilleke SC. The response of guinea pig
652 primary utricular and saccular irregular neurons to bone-conducted vibration (BCV) and air-
653 conducted sound (ACS). *Hear Res* (2016) 331:131-43. doi: 10.1016/j.heares.2015.10.019.
654 116. Highstein SM, Mann MA, Holstein GR, Rabbitt RD. The quantal component of synaptic
655 transmission from sensory hair cells to the vestibular calyx. *J Neurophysiol* (2015) 113(10):3827-
656 35. doi: 10.1152/jn.00055.2015.
657 117. Sadeghi SG, Pyott SJ, Yu Z, Glowatzki E. Glutamatergic signaling at the vestibular hair cell
658 calyx synapse. *J Neurosci* (2014) 34(44):14536-50. Epub 2014/10/31. doi:
659 10.1523/jneurosci.0369-13.2014.
660 118. Ramachandran S, Rodgriguez S, Potcoava M, Alford S. Single calcium channel
661 nanodomains drive presynaptic calcium entry at lamprey reticulospinal presynaptic terminals. *J*
662 *Neurosci* (2022). Epub 2022/01/23. doi: 10.1523/JNEUROSCI.2207-21.2022.
663 119. Art JJ, Wu YC, Fettiplace R. The calcium-activated potassium channels of turtle hair cells. *J*
664 *Gen Physiol* (1995) 105(1):49-72. Epub 1995/01/01.
665